

SegMatch: A semi-supervised learning method for surgical instrument segmentation

Meng Wei[†] Charlie Budd[†] Luis C. Garcia-Peraza-Herrera[†] Reuben Dorent^{†+}

Miaoqing Shi^{†‡} Tom Vercauteren[†]

[†]King's College London

[‡]Tongji University

⁺Harvard Medical School

{first_name}.{last_name}@kcl.ac.uk

Abstract

Surgical instrument segmentation is recognised as a key enabler to provide advanced surgical assistance and improve computer-assisted interventions. In this work, we propose SegMatch, a semi-supervised learning method to reduce the need for expensive annotation for laparoscopic and robotic surgical images. SegMatch builds on FixMatch, a widespread semi-supervised classification pipeline combining consistency regularization and pseudo-labelling, and adapts it for the purpose of segmentation. In our proposed SegMatch, the unlabelled images are weakly augmented and fed into the segmentation model to generate a pseudo-label to enforce the unsupervised loss against the model's output for the adversarial-augmented image on the pixels with a high confidence score. Our adaptation for segmentation tasks includes carefully considering the equivariance and invariance properties of the augmentation functions we rely on. To increase the relevance of our augmentations, we depart from using only handcrafted augmentations and introduce a trainable adversarial augmentation strategy. Our algorithm was evaluated on the MICCAI Instrument Segmentation Challenge datasets Robust-MIS 2019 and EndoVis 2017. Our results demonstrate that adding unlabelled data for training purposes allows us to surpass the performance of fully supervised approaches which are limited by the availability of training data in these challenges. SegMatch also outperforms a range of state-of-the-art semi-supervised learning semantic segmentation models in different labelled to unlabelled data ratios.

1. Introduction

Automatic visual understanding in laparoscopic and robotic surgical videos is crucial for enabling autonomous surgery and providing advanced surgical support to clinical

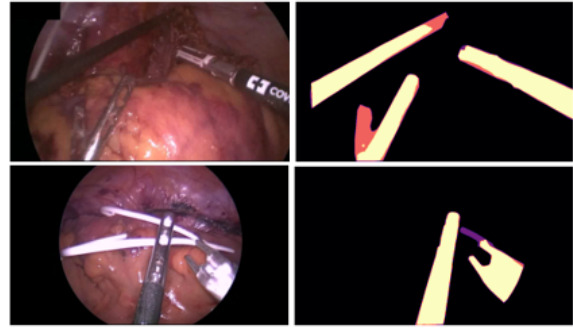


Figure 1. Representative sample images from Robust-MIS 2019 of laparoscopic surgery (left) and state-of-the-art instrument segmentation results (right). True positive (yellow), true negative (black), false positive (purple), and false negative (red).

cal teams. Within this field, instrument segmentation, as shown in Figure 1, is a fundamental building block. Example use cases include automatic surgical skill assessment, placing informative overlays on the display, performing augmented reality without occluding instruments, intra-operative guidance systems, surgical workflow analysis, visual servoing, and surgical task automation [37]. Surgical instrument segmentation has advanced rapidly from traditional methods [45, 35], to modern deep learning-based methods [22, 15, 18, 28, 17]. Given the significance of this task, open datasets have been released, in particular, through the organisation of computational challenges such as Robust-MIS 2019 [37].

Most studies in this area exploit fully supervised learning, the performance of which scales with the amount of labelled training data. However, given the required expertise to provide accurate manual segmentation, the collection of annotations is costly and time-consuming. It is thus unsurprising that in comparison to industry standards for natural images, no large-scale annotated datasets for surgical tool

segmentation currently exist. This leads to significant barriers in establishing the robustness and precision needed to deploy surgical instrument segmentation in the clinic. To tackle this challenge, a number of weak supervision approaches [39, 38, 25, 41, 50] have been proposed which take advantage of unlabelled data or image-level labels as these are easier to capture. While interesting conceptually, weak supervision for surgical instrument segmentation has not yet been demonstrated in practice to generalize to large-scale datasets and achieve the required accuracy for deployment in the operating theatre.

In this work, we propose a new semi-supervised surgical instrument segmentation framework, termed as SegMatch, building upon the state-of-the-art semi-supervised image *classification* pipeline, FixMatch [43]. During training, FixMatch processes unlabelled input images through two concurrent paths which implement weak (*e.g.* image flip and rotation) and strong (*e.g.* significant photometric changes) augmentations respectively. Augmented images from both paths are then fed to a shared backbone prediction network. For regions of high confidence, the prediction from the weakly augmented image serves as a pseudo-ground-truth against which the strongly augmented image is compared.

In order to adapt FixMatch to the segmentation task, we make a seemingly small but critical first contribution by changing the augmentation paths in SegMatch. For classification tasks, networks are expected to be invariant with respect to all types of augmentation within a certain range tailored to the specific requirements of the task. In contrast, for segmentation tasks, networks are expected to be invariant with respect to photometric transformations (*e.g.* contrast, brightness, hue changes) but equivariant with respect to spatial transformations (*e.g.* rotations, translations, flips). In SegMatch, spatial transformations that are used as augmentations are inverted after the network prediction.

Our second and main contribution to SegMatch lies in the inclusion of a learned strong augmentation strategy. Promoting prediction consistency between the weakly augmented and strongly augmented branches is what helps FixMatch and SegMatch learn from unlabelled data and generalise better. Yet, there is no guarantee that the fixed, hand-crafted set of strong augmentation types suggested in [43] is optimal. In fact, once the network learns to be sufficiently invariant/equivariant with respect to the fixed set of augmentation, the information learned from the unlabelled data would have saturated. In order to guide the model to learn continuously as the training progresses, we introduce an adversarial augmentation scheme to generate strongly augmented data. We rely on the established iterative fast gradient sign method (I-FGSM) [21] and integrate it into our training loop to dynamically adapt the strong augmentation as we learn from the data.

We conduct extensive experiments on both the Robust-MIS 2019 [37] and EndoVis 2017 datasets [1]. Our study demonstrated that using a ratio of 1:9 or 3:7 of labelled data to unlabelled data within a dataset allowed our model to achieve a considerably higher mean Dice score compared to state-of-the-art semi-supervised methods. Our method shows a significant improvement in surgical instrument segmentation compared to existing fully supervised methods by utilizing a selective set of 17K unlabelled images available in the Robust-MIS 2019 dataset in addition to the annotated subset which most competing methods have exploited.

2. Related work

2.1. Semi-supervised learning

Pseudo-labelling [49, 32] is a representative approach for semi-supervised learning. A model trained on labelled data is utilized to predict pseudo-labels for unlabelled data. This in turn provides an extended dataset of labelled and pseudo-labelled data for training. Consistency regularization [47, 34] is also a widespread technique in semi-supervised learning. There, an auxiliary objective function is used during training to promote consistency between several model predictions, where model variability arises from techniques such as weight smoothing or noise injection.

Berthelot *et al.* [4] introduced MixMatch to incorporate both consistency regularization and the Entropy Minimization strategy of Granvalet and Bengio [14] into a unified loss function for semi-supervised image classification. Aiming at providing a simple yet strong baseline, Sohn *et al.* [43] introduced FixMatch to combine consistency regularization and pseudo-labelling and achieve state-of-the-art performance on various semi-supervised learning benchmarks.

Semi-supervised semantic segmentation: Adapting semi-supervised learning for image segmentation tasks requires dedicated strategies that account for the fact that labels are provided at the pixel level. Previous works explored the adaptation to semantic segmentation of classical semi-supervised learning including pseudo-labelling [20, 24], and consistency regularization [10, 6]. Ouali *et al.* [30] proposed cross-consistency training (CCT) to force the consistency between segmentation predictions of unlabelled data obtained from a main decoder and those from auxiliary decoders. Similarly, Chen *et al.* [7] exploited a novel consistency regularization approach called cross pseudo-supervision such that segmentation results of variously initialised models with the same input image are required to have high similarity. Previous work also investigated the use of generative models to broaden the set of unlabelled data from which the segmentation model can learn [44].

Despite such advances, current semi-supervised semantic segmentation models derived from classification models

have not yet demonstrated the performance gains observed with FixMatch for classification. We hypothesise that an underpinning reason is that they do not adequately address the issue of transformation equivariance and invariance and do not exploit modern augmentation strategies as efficiently as FixMatch.

2.2. Surgical instrument segmentation

The majority of surgical instruments segmentation works are supervised methods [18, 12, 28, 33, 19, 42]. Numerous studies have explored different methods to improve the accuracy of surgical instrument segmentation. For instance, Islam *et al.* [18] took advantage of task-aware saliency maps and the scan path of instruments in their multitask learning model for robotic instrument segmentation. By using optical flow, Jin *et al.* [19] derived the temporal prior and incorporate it into an attention pyramid network to improve the segmentation accuracy. Recently, Gonzalez *et al.* [12] proposed an instance-based surgical instrument segmentation network (ISINet) with a temporal consistency module that takes into account the instance’s predictions across the frames in a sequence. Seenivasan *et al.* [42] exploited global relational reasoning for multi-task surgical scene understanding which enables instrument segmentation and tool-tissue interaction detection. Yet, the use of unlabelled data for this task remains relatively untapped.

Surgical instrument segmentation with limited supervision: A relatively small number of works exploited surgical instrument segmentation with limited supervision. Jin *et al.* [19] transferred predictions of unlabelled frames to that of their adjacent frames in a temporal prior propagation-based model. Liu *et al.* [25] proposed an unsupervised approach that relies on handcrafted cues including color, object-ness, and location to generate pseudo-labels for background tissues and surgical instruments respectively. More recently, Sanchez *et al.* [41] used image-level labels in a multi-task learning framework to jointly detect and segment surgical instruments. Sahu *et al.* [39] relies on inherently annotated simulation data and unlabelled real data to train a teacher-student model for simulation-to-real domain adaptation in endoscopic image segmentation. Liu *et al.* [26] introduced a graph-based unsupervised method for adapting a surgical instrument segmentation model to a new domain with only unlabelled data.

We note that most of the existing works with limited supervision focus on exploring domain adaptation or generating different types of pseudo-labels for surgical tool segmentation models and do not exploit a FixMatch-style semi-supervised learning.

2.3. Adversarial learning for improved generalisation

Deep neural networks (DNNs) have been found to be vulnerable to some well-designed input samples, known as adversarial samples. Adversarial perturbations are hard to perceive for human observers, but they can easily fool DNNs into making wrong predictions. The study of adversarial learning concerns two aspects: 1) how to generate effective adversarial examples to attack the model [13]; 2) how to develop efficient defence techniques to protect the model against adversarial examples [16]. A model which is robust to adversarial attacks is also more likely to generalise better [2]. As such, we hypothesise that adversarial methods may be of relevance for semi-supervised learning.

For adversarial attacks, the earliest methods [46, 13] rely on the gradient of the loss with respect to the input image to generate adversarial perturbations. For instance, fast gradient sign attack (FGSM) [46] perturbs the input along the gradient direction of the loss function to generate adversarial examples. Tramèr *et al.* [48] improved the FGSM by adding a randomization step to escape the non-smooth vicinity of the data point for better attacking. The basic iterative method (BIM) [21], which is also referred to as iterative FGSM (I-FGSM), improves FGSM by performing multiple smaller steps to increase the attack success rate. Carlini *et al.* [5] introduced a method now referred to as C&W which solves a constrained optimisation problem minimising the size of the perturbation while ensuring a wrong prediction after perturbation. Recently, Rony *et al.* [36] proposes a more efficient approach to generate gradient-based attacks with low L2 norm by decoupling the direction and norm (DDN) of the adversarial perturbation. For adversarial defence, adversarial training [27] is a seminal method which generates adversarial examples on the fly and trains the model against them to improve the model’s robustness. Other defence methods include relying on generative models [40] and leveraging the induced randomness to mitigate the effects of adversarial perturbations in the input domain [8].

Although the adversarial attack has the potential to enhance the performance and robustness of deep learning models, it has not been yet applied to semi-supervised learning methods for semantic segmentation. As we show later in this work, adversarial attacks can indeed be used to effectively augment unlabelled images used for consistency optimization.

3. Methods

3.1. Proposed SegMatch algorithm: overview

Our proposed SegMatch algorithm adapts the state-of-the-art semi-supervised image *classification* framework, FixMatch [43], to semi-supervised semantic *segmentation*.

Our application primarily targets the segmentation of surgical instruments but also has the potential to be utilized for various other semantic segmentation tasks. We follow the basic architecture of FixMatch as illustrated in Figure 2. During training, SegMatch uses a supervised pathway and an unsupervised pathway which share the same model parameters θ for segmentation prediction. For the supervised pathway, the prediction from the labelled image is classically optimized against its ground truth using a standard supervised segmentation loss. For the unsupervised pathway, given an unlabelled image, we follow FixMatch and process the input image through two concurrent paths, which implement weak and strong augmentations respectively. The augmented images are then fed to the model to obtain two segmentation proposals. The output from the weak augmentation branch is designed to act as the pseudo-ground-truth for that from the strong augmentation branch.

As detailed in Section 3.2, segmentation models are typically expected to be invariant with respect to bounded photometric transformations and equivariant with respect to spatial transformations of the input images. We use simple spatial transformations for our weak augmentations and propose to apply the inverse spatial transformation after the network prediction to handle spatial transformation equivariance. We use photometric transformations for our strong augmentations and exploit a pixel-wise loss promoting consistency between the segmentation outputs of the two branches.

Given the complexity of determining the suitable range of parameters for hand-crafted strong augmentation, we propose a solution that involves a learning-based approach. As detailed in Section 3.3, in order to gradually increase the difficulty of the prediction from the strongly-augmented branch, we introduce a learnable adversarial augmentation scheme in the strong augmentation branch.

3.2. Weak augmentations, equivariance, pseudo-labels

Equivariance and invariance in SegMatch: We start by introducing the notion of equivariance and invariance illustrated in Figure 3. Let us consider a function f_θ (standing for the neural network, θ being the parameters of the network) with an input x (standing for the input image), and a class of transformation functions \mathcal{G} (standing for a class of augmentations). If applying $g \in \mathcal{G}$ (standing for a specific augmentation instance) to the input x also reflects on the output of f_θ , that is $f_\theta(g(x)) = g(f_\theta(x))$, then the function f_θ is said to be equivariant with respect to transformations in \mathcal{G} (see Figure 3: Left). Conversely, if applying $g \in \mathcal{G}$ to the input x does not affect the output of f_θ , that is $f_\theta(g(x)) = f_\theta(x)$, then the function f_θ is said to be invariant with respect to transformations in \mathcal{G} (see Figure 3: Right).

For the classification task, the model is expected to be invariant to all the augmentation strategies. In contrast, given a segmentation model, spatial transformations on the input image should reflect on the output segmentation map while photometric transformations should not. Segmentation models should thus be equivariant with respect to spatial transformations and invariant with respect to photometric transformation. In FixMatch, weak augmentations only comprise simple spatial transformations such as rotation, and flip, which preserve the underlying structure of the image. Meanwhile, strong augmentations only comprise photometric transformations such as posterizing and sharpness changes as provided by the RandAugment [9] algorithm, which shifts the intensity distribution of the original image.

Inverting transformations from the weak augmentations: Similar to FixMatch, given an input unlabelled image, we randomly select one simple spatial transformation, *i.e.* rotation, flip, crop or resize, to apply to it in the weak augmentation branch. In order for our SegMatch to take advantage of a consistency loss between the weak augmentation branch where spatial transformations are used (with expected equivariance of the segmentation) and the strong augmentation branch where photometric transformations are used (with expected invariance of the segmentation), we deploy an inverse spatial transformation on the output of the segmentation model in the weak augmentation branch.

Given an unlabelled image x^u , we denote its weak augmentation as $\omega_e(x^u)$. It is fed to the network f_θ to obtain the segmentation output $f_\theta(\omega_e(x^u))$. We apply the inverse transformation ω_e^{-1} to $f_\theta(\omega_e(x^u))$, *i.e.* $\omega_e^{-1}(f_\theta(\omega_e(x^u)))$. This addresses the equivariance expectation and allows for the output of the weak augmentation branch to be easily compared with the segmentation output from the strongly-augmented image.

Soft pseudo-label generation: Following the inverse transformation, we obtain a segmentation prediction in logit space $p_w = \omega_e^{-1}(f_\theta(\omega_e(x^u)))$. For the i -th pixel in p_w , *i.e.* p_{w_i} , a pseudo-label is extracted by applying a sharpened softmax:

$$\tilde{y}_i = \text{Sharpen}(\text{Softmax}(p_{w_i}), T) \quad (1)$$

where the distribution sharpening operation of [4] is defined as $\text{Sharpen}(d, T)_i := d_i^{\frac{1}{T}} / \sum_{j=1}^L d_j^{\frac{1}{T}}$. with T being a temperature hyper-parameter. The sharpening operation allows us to control the level of confidence in the resulting probabilities.

3.3. Trainable strong augmentations

To tackle the generalization problem typically faced by convolutional neural networks, previous work has em-

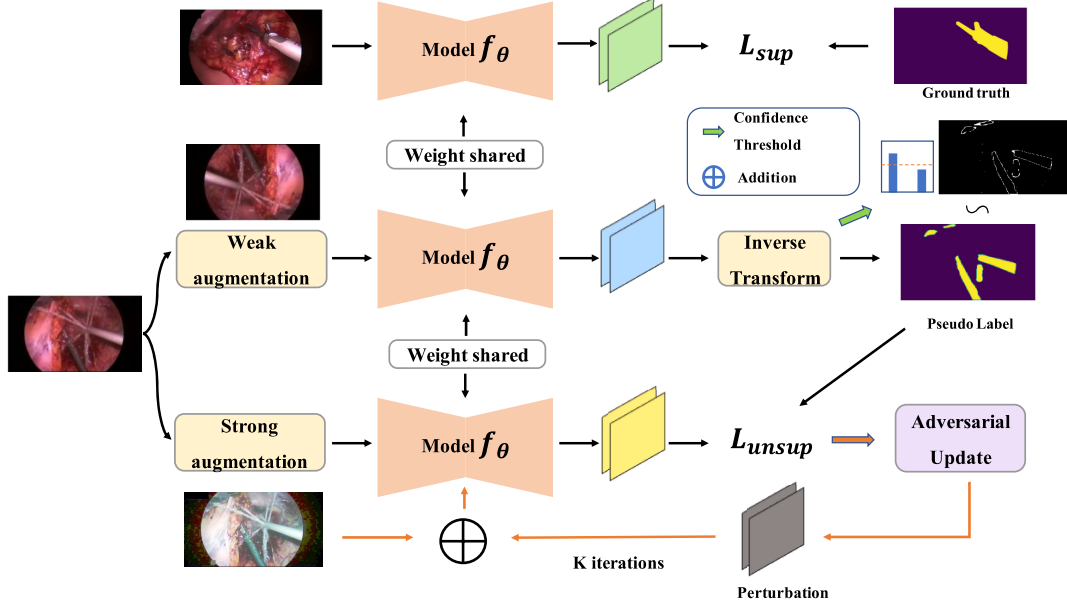


Figure 2. SegMatch training process structure. The top row is the fully supervised pathway which follows the traditional segmentation model training process. The two bottom rows form the unsupervised learning pathway, where one branch uses a weakly augmented image fed into the model to compute predictions, and the second branch obtains the model prediction via strong augmentation for the same image. The model parameters are shared across the two pathways. The hand-crafted photometric augmentation methods are used to initialize the strong augmented image, which is further perturbed by an adversarial attack (I-FGSM) for K iterations.

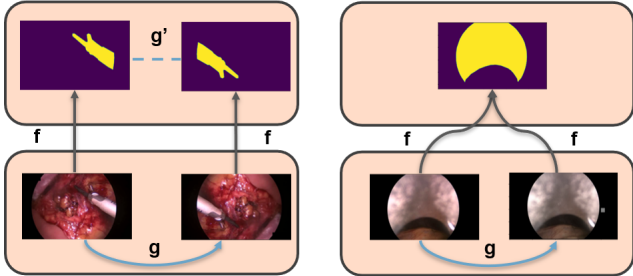


Figure 3. Equivariance (left) and invariance (right) properties for an image augmented under different types of augmentations: spatial (left) or photometric (right).

employed strong augmentations techniques [43, 4, 3]. However, these augmentations are hand-crafted and designing realistic strong augmentations to bridge large and complex domain gaps is challenging [11]. This challenge is further exacerbated in segmentation tasks which are highly sensitive to pixel-level perturbations due to their pixel-level prediction nature[29]. For these reasons, despite utilizing powerful hand-crafted augmentations during training, existing methods still demonstrate limited generalization capabilities. In this section, we propose to tackle these key limitations by learning to perform data augmentation using adversarial perturbation during model training.

Strong Augmentation Initialization: Rather than completely replacing the strong augmentation approach in Fix-

Match, we build on it to serve as initialization which will be further perturbed. We chose the strong augmentations from the operations in RandAugment [9] based on two criteria. First, we focus on photometric transformations only as these satisfy the invariance expectation and do not require the use of an inverse transformation as discussed in Section 3.2. Second, we select rather basic transformations that provide visually plausible augmentations, thereby leaving the more complex changes to the trainable refinement. More specifically, our initial augmentation for the strong augmentation branch is a composition of three transformations randomly chosen from a collection of handcrafted photometric augmentation strategies. These include adjustments to contrast, brightness, colour, and sharpness, as well as the addition of random noise, posterization, and solarization. The strength of the individual transformations is chosen according to predefined hyper-parameters.

Adversarial augmentation approach: As a simple yet powerful adversarial method, we decide to use the iterative fast gradient sign method (I-FGSM) [21], which applies multiple gradient updates by iterative small steps.

I-FGSM is based on FGSM which provides an adversarial perturbation to the input image in a single gradient-based operation. In FGSM, the direction of the perturbation is computed from the gradient of the loss with respect to the input image. The magnitude of the gradient is discarded by keeping only the sign along each dimension. A scaling factor is applied to keep the perturbation small. To compute

a more refined perturbation, I-FGSM applies FGSM multiple times in smaller steps. The perturbations are clipped to make sure they are in the ϵ -neighbourhood to the original image. The I-FGSM equation for iteration $k + 1$ out of K is as follows:

$$x_{k+1}^s = \text{Clip}_{x_0^s, \epsilon} \left\{ x_k^s + \frac{\epsilon}{K} \cdot \text{Sign}(\nabla_{x_k^s} (L_u(f_\theta(x_k^s), \tilde{y})) \right\} \quad (2)$$

where x_0^s represents the initial strongly-augmented image; \tilde{y} is the pseudo-label obtained from the weak augmentation branch; $\text{Clip}\{\cdot\}$ is the clipping function which applies to every pixel in the perturbation image to limit the difference between x_K^s and x_0^s and keep it within an ϵ -neighbourhood; and L_u is the unsupervised loss function defined in equation (4). The magnitude of the perturbation ϵ and the number of I-FGSM steps K are hyperparameters to adjust the quality of the adversarial approach.

3.4. Loss functions in SegMatch

In this work, the training objective for the supervised pathway is the standard pixel-wise cross-entropy loss (l_{CE}) combined with Dice loss ($l_{DSC} = 1 - DSC$), where DSC represents the Dice coefficient:

$$L_s = \frac{1}{|\mathcal{D}^l|} \sum_{x^l \in \mathcal{D}^l} \left(l_{DSC}(y^l, f_\theta(x^l)) + \frac{1}{N} \sum_{i=0}^{N-1} l_{CE}(y_i^l, f_\theta(x^l)_i) \right) \quad (3)$$

where x^l is a labelled input from the labelled set \mathcal{D}^l ; y^l is the corresponding ground-truth label; x_i^l and y_i^l denote the i^{th} pixel of x^l and y^l , respectively; and N is the number of pixels in x^l .

The training objective for the unsupervised pathway is a cross-entropy loss calculated between a subset of confident pixel-level pseudo-labels \tilde{y}_i stemming from the weak augmentation branch and the output probability p_i from the strongly augmented image:

$$L_u = \frac{1}{|D_u|} \sum_{x^u \in D_u} \frac{1}{|N_v^{x^u}|} \sum_{i \in N_v^{x^u}} l_{CE}(\tilde{y}_i, p_i) \quad (4)$$

where x^u is an unlabelled input from the unlabelled set \mathcal{D}^u ; c denotes a specific class; and $N_v^{x^u}$ is the set of pixel indices with confidence score of the most confident class $\max_c(p_{w_i}^c)$ higher than or equal to a hyper-parameter threshold t , i.e. $N_v^{x^u} = \{i \mid \max_c(p_{w_i}^c) \geq t\}$.

The final loss is given by:

$$L = L_s + w(t)L_u \quad (5)$$

where, following [23], $w(t)$ is an epoch-dependent weighting function which starts from zero and ramps up along a Gaussian curve so that the supervised loss contributes to the total loss more at the beginning and the unsupervised loss increases contribution in subsequent training epochs.

4. Experimental setup

4.1. Dataset

Robust-MIS 2019: Robust-MIS 2019 is a laparoscopic instruments dataset including procedures in rectal resection, proctocolectomy, and sigmoid resection to detect, segment, and track medical instruments based on endoscopic video images [37]. The training data encompasses 10-second video snippets in the form of 250 consecutive endoscopic image frames and the reference annotation for only the last frame is provided. In total, 10,040 annotated images are available from a total of 30 surgical procedures from three different types of surgery.

As per the original challenge, the samples used for training were exclusively taken from the proctocolectomy and rectal resection procedures. These samples comprise a total of 5983 clips, with each clip having only one annotated frame while the remaining 249 frames are unannotated.

The testing set is divided into three phases as per the original challenge, where there was no patient overlap between the training and test datasets. *Stage 1:* 325 images from the proctocolectomy procedure with another 338 images from the rectal resection procedure. *Stage 2:* 225 images from the proctocolectomy procedure and 289 others from the rectal resection procedure. *Stage 3:* 2880 annotated images from sigmoid resection, an unknown surgery which only appears in the testing stage but not in the training stage.

EndoVis 2017: EndoVis 2017 is a robotic instrument image dataset captured from robotic-assisted minimally invasive surgery [1], which comprises a collection of 10 recorded sequences capturing abdominal porcine procedures. For the training phase, the first 225 frames of 8 sequences were captured at a rate of 2Hz and manually annotated with information on tool parts and types. The testing set consists of the last 75 frames from the 8 sequences used in the training data videos, along with 2 full-length sequences of 300 frames each, which have no overlap with the training phase. To prevent overlap between the training and test sets from the same surgical sequence, we followed the same split as described in ISINet [12]. This involved exclusively assigning the 2 full-length sequences for testing while keeping the training set intact with 225 frames from the remaining 8 sequences. Note that there are no additional unannotated images for EndoVis 2017.

Dataset usage for semi-supervised learning evaluation: Since the above challenges were designed for fully supervised benchmarking, we make some adaptations to evaluate SegMatch with respect to competitive semi-supervised (and fully supervised) methods.

The Robust-MIS 2019 dataset was split into training and testing sets based on the original challenge splits. The three original challenge testing stages were merged to form a sin-

gle combined testing set, comprising 4057 images. For training, we started with the full set of 5,983 labelled original challenge training images and the corresponding 17,617 unlabelled images. In our first experiments, we use only the 5,983 labelled original challenge training images and keep only 10% or 30% of the annotations. This allows for a comparison with supervised methods having access to all 5983 labelled images. To further compare with the state-of-the-art supervised methods, we also conducted experiments using the whole 5,983 images of the training set as a labelled set, and use 17,617 additional unlabelled frames from the original videos.

For EndoVis 2017, as no additional unlabeled data is available, the original training set, which has 1800 images in total, is split into labelled and unlabelled subsets with ratios 1:9 or 3:7.

4.2. Implementation details

During training, for each batch, the same number of images is sampled from the labelled dataset D_l and the unlabelled dataset D_u . Within each batch, unlabelled samples are initialized by random but hand-crafted strong augmentations and then adversarially updated by adding the I-FGSM perturbation.

All our experiments were trained on two NVIDIA V100 (32GB) with a learning rate of 0.001. The model was trained using an SGD optimizer with a momentum of 0.95, which we found can provide a smooth convergence trajectory (unreported manual tuning involved experiments with momentum values from 0.9 to 0.99). The learning rate was initialized as 1.0×10^{-2} and decayed with the policy $lr_{ini} \times (1 - epoch/epoch_{max}) \times \eta$, where $epoch_{max}$ is the total epochs and η is set to 0.7. The total training epoch number is 1000 and the batch size was set as 64 considering the memory constraints and training efficiency.

In the final model, adversarial augmentation was applied with a magnitude of $\epsilon = 0.08$. Additionally, two types of initial strong augmentation techniques were utilized with pre-defined minimum and maximum magnitude values, specifically from the photometric transformations in RandAugment [9] method.

For the segmentation model backbone, we employed the state-of-the-art OR-Unet [17]. Our OR-Unet contains 6 downsampling and 6 upsampling blocks where the residual blocks were employed in the encoder and the sequence Conv-BN-Relu layers with kernel size 3×3 were used in the decoder.

4.3. Evaluation metrics

We evaluated our model based on the criterion proposed in Robust-MIS 2019 MICCAI challenge [37], which includes:

- Dice Similarity Coefficient, a widely used overlap metric in segmentation challenges;
- Normalized Surface Dice (NSD) [37] is a distance-based measurement for assessing performance, which measures the overlap of two surfaces (i.e. mask borders). In adherence to the challenge guidelines [37], we set the tolerance value for NSD to 13 pixels, which takes into account inter-rater variability. Note that the value of tolerance was determined by comparing annotations from five annotators on 100 training images as illustrated in the challenge.

5. Results and discussion

5.1. Comparison With State-of-the-Art Models

We compare our results to the state-of-the-art on Robust-MIS 2019 and EndoVis 2017 datasets. We categorize comparisons into two groups. First, a head-to-head comparison is made with other semi-supervised methods. Second, we measure the added value of incorporating unlabelled data in addition to using the complete labelled training data in Robust-MIS 2019.

Comparison with semi-supervised baselines: For the first group, we adapted the representative semi-supervised classification method Mean-Teacher [47] for the segmentation task using the same backbone network and experimental setting as ours. We also conducted experiments using two existing semi-supervised semantic segmentation models: WSSL [31], and CCT [30]. WSSL is an established yet representative benchmark for semi-supervised semantic segmentation. CCT ensures consistency among high-level features with different contexts, which is accomplished by aligning perturbed features with the main features. The motivation behind CCT is thus similar to ours while CCT requires several decoders and additional computational resources. Illustrative segmentation results for the above methods on Robust-MIS 2019 are presented in Figure 4.

Table 1 shows that, within the dataset of Robust-MIS 2019, for the two labelled to unlabelled data ratios we tested, our SegMatch outperforms other methods with statistical significance ($p < 0.05$). Comparing SegMatch to the second-best method, CCT, we observed notable improvements in performance. Specifically, when using 10% and 30% labelled data in the Robust-MIS 2019 dataset, SegMatch achieved mean Dice score improvements of 6.2 percentage points (pp) and 9.1 pp, respectively. Similar observations were made on the EndoVis 2017 dataset, where SegMatch outperformed CCT by 4 pp and 4.6 pp when utilizing 10% and 30% labelled data, respectively.

These results demonstrate the superior performance of SegMatch in both datasets and both labelled to unlabelled data ratios, highlighting the effectiveness of our proposed method in scenarios with limited labelled data. Note that,

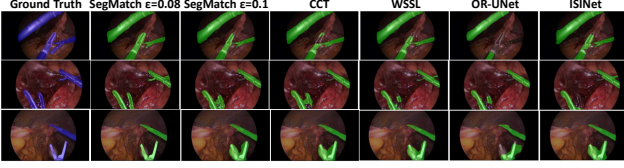


Figure 4. Segmentation results on exemplar images from three different procedures in the testing set. Here, SegMatch, CCT, and WSSL were trained using the whole labelled training set of Robust-MIS 2019 as a labelled set, and 17K additional unlabelled frames from the original videos. The fully supervised learning models (OR-UNet and ISINet) were trained using the whole labelled training set of Robust-MIS 2019 as a labelled set. The first column is the ground truth mask placed on the top of the original image, and the other column is the segmentation results of ablation models of SegMatch and state-of-the-art models. The three rows from up to bottom are the testing image samples from proctocolectomy procedures, sigmoid resection procedure (unseen type), and rectal resection procedure respectively.

the training dataset only consists of the proctocolectomy procedure and rectal resection procedure, and the sigmoid resection procedure is considered a new type of data for the trained model. Qualitatively, our proposed SegMatch is able to recognize the boundaries between different tools and segment more complete shapes for each individual tool, especially in those areas with high reflection.

Added value of unlabelled data: For the second group, we used the whole labelled training set of Robust-MIS 2019 as the labelled set and take advantage of the unlabelled video footage available from the training set of Robust-MIS 2019 to evaluate the impact of adding unlabelled data to an already large labelled dataset. We include 17,617 randomly selected unlabelled images from the training clips as the unlabelled set.

Table 2 shows the comparison between supervised approaches trained on the labelled set and SegMatch trained on the combination of the labelled and unlabelled sets. Compared to the existing model OR-UNet [17], the inclusion of additional unlabelled data in our semi-supervised pipeline SegMatch led to a 5.7 pp higher Dice score. Our model also demonstrates a noteworthy enhancement of 4.8 pp in comparison to the more recent ISINet [12], which is now commonly employed for surgical instrument segmentation. When evaluating the stage 3 testing data, which corresponds to a surgical procedure that was not seen during the training phase, our SegMatch model demonstrated superior performance compared to the official Robust-MIS 2019 challenge winner for stage 3 (haoyun team) by a margin of 3.9 pp. It is noteworthy that the performance improvement from SegMatch over fully supervised baselines is more substantial on stage 3 testing data (unseen procedure types) than on stage 1 and 2 data (procedure types represented in the training data). This indicates that our model exhibits

better generalizability. This enhanced generalizability can enable the model to handle diverse surgical scenarios more effectively.

5.2. Ablation and parameter sensitivity study

To evaluate the contribution of the different components of our pipeline, we conducted ablation and parameter sensitivity studies on different strong augmentation strategies and adversarial strong augmentation methods.

Analysis of our semi-supervised method: We evaluate the contribution of the semi-supervised learning in SegMatch by training only its fully-supervised branch, essentially turning it into OR-UNet. As discussed previously and shown in Table 2, disabling the unlabelled pathway leads to a drop in terms of Dice and NSD scores thereby confirming the benefits of semi-supervised learning.

We also studied the effectiveness of varying the confidence threshold when generating the pseudo-labels as shown in Figure 5. We observe that when the confidence threshold approaches 1.0, the model returns the worst segmentation performance. When the threshold value is changed within the range of [0.7, 0.9], the confidence threshold does not affect the model’s performance significantly. However, it should be noted that further reducing the threshold value leads to a rapid decrease in the mean Dice score, which indicates that the quality of contributing pixels to the unsupervised loss may be more important than the quantity.

Augmentation strategy: We also operated an ablation study on the weak and strong augmentation in SegMatch as tabulated in Table 3. First, we removed the adversarial augmentation, thereby only keeping handcrafted strong augmentations. Notably, we observed consistent results across different labelled data ratios. Specifically, when utilizing 17K additional unlabelled data, we found that the Dice score decreased by 3.1 pp compared to the full proposed SegMatch model. This suggests that applying adversarial augmentations can prevent the learning saturation caused by handcrafted strong augmentations on unlabelled data, thereby enabling the model to learn continuously. When both the weak augmentation and adversarial augmentation are removed, the results drop by an additional 1.9 pp compared to only removing the adversarial augmentation, indicating that applying the weak augmentation function to the input image, which generates new and diverse examples for the training dataset, can enhance the segmentation performance.

To evaluate the effectiveness of the overall strong augmentation strategies, we replaced the strongly augmented images with the original images. The resulting Dice score dropped by 5.1 pp compared to only removing the adversarial augmentation, and by 3.2 pp compared to removing both the weak and adversarial augmentation. The evidence that

Table 1. State-of-the-art semi-supervised model comparisons for Robust-MIS 2019 dataset (left) and EndoVis 2017 dataset (right) under differently labelled data to unlabelled data ratio

| Methods | Robust-MIS 2019 (5983 training images) | | | | EndoVis 2017 (5286 training images) | | | |
|-------------------|--|-----------------|----------------------|-----------------|-------------------------------------|-----------------|----------------------|-----------------|
| | Labelled: 598 (10%) | | Labelled: 1794 (30%) | | Labelled: 528 (10%) | | Labelled: 1585 (30%) | |
| | Mean Dice | NSD | Mean Dice | NSD | Mean Dice | NSD | Mean Dice | NSD |
| Mean-teacher [47] | 62.1 | 61.8 | 70.2 | 69.0 | 51.6 | 52.7 | 60.2 | 59.9 |
| WSSL[31] | 64.3 | 62.6 | 72.1 | 73.2 | 59.2 | 60.4 | 67.5 | 70.2 |
| CCT[30] | 67.1 | 65.2 | 75.2 | 72.6 | 61.2 | 58.7 | 69.6 | 65.5 |
| SegMatch | 73.3 \pm 0.42 | 71.2 \pm 0.48 | 84.3 \pm 0.61 | 80.2 \pm 0.51 | 65.2 \pm 0.26 | 66.3 \pm 0.42 | 74.2 \pm 0.33 | 71.0 \pm 0.45 |

Table 2. Comparison on the Robust-MIS 2019 dataset between fully supervised models and SegMatch with additional unlabelled data. (* indicates only labelled data was used)

| Method | Labelled: 5983 training images (+17K unlabelled if semi-supervised) | | | | | | | |
|------------------------------|---|-----------------|-----------------|-----------------|-----------------|-----------------|-----------------|-----------------|
| | Whole Testing | | Stage 1 | | Stage 2 | | Stage 3 | |
| | Mean Dice | NSD | Mean Dice | NSD | Mean Dice | NSD | Mean Dice | NSD |
| OR-Unet [17]* | 88.0 | 86.2 | 90.2 | 88.5 | 87.9 | 85.6 | 85.9 | 84.5 |
| Robust-MIS 2019 winner [37]* | 90.1 | 88.9 | 92.0 | 92.7 | 90.2 | 88.6 | 89.0 | 86.4 |
| ISINet [12]* | 88.9 | 86.3 | 90.9 | 87.6 | 89.6 | 86.5 | 86.2 | 84.7 |
| SegMatch | 93.7 \pm 0.28 | 93.6 \pm 0.24 | 95.1 \pm 0.23 | 95.5 \pm 0.19 | 93.1 \pm 0.49 | 92.5 \pm 0.31 | 92.9 \pm 0.12 | 92.8 \pm 0.22 |

Table 3. Ablation study results for different components, evaluating on Robust-MIS 2019 with different labelled and unlabelled data amount

| Method | Labelled: 1794 (30%) | | Labelled: 5983 (+17K unlabelled) | |
|--------------------------------|----------------------|------|----------------------------------|------|
| | Mean Dice | NSD | Mean Dice | NSD |
| SegMatch (proposed) | 84.3 | 80.2 | 93.7 | 93.6 |
| No adversarial | 80.6 | 77.9 | 90.6 | 89.9 |
| No adversarial & No weak aug | 75.6 | 73.7 | 88.7 | 87.6 |
| No adversarial & No strong aug | 71.5 | 68.2 | 85.5 | 86.9 |

removing strong augmentation results in a greater decrease in performance than removing weak augmentation suggests that stronger perturbations are beneficial for learning with consistency regularization. Additionally, when strong augmentation is removed, the model is presented with the same input image from different views, which reduces the benefits of consistency regularization. In this scenario, pseudo-labelling becomes the primary technique for achieving better segmentation performance. Therefore, our results suggest that consistency regularization is more crucial than pseudo-labelling in our pipeline for improving segmentation performance.

Adversarial augmentation analysis: We further evaluated the sensitivity of our results to changes in the maximum amplitude value ϵ of the adversarial perturbation as shown in Figure 6 and qualitatively illustrated in Figure 7. When increasing from $\epsilon = 0.0$ (i.e. no perturbation), we observed a consistent pattern across different ratios of labelled data for both FGSM and I-FGSM. Initially, as ϵ increased, the segmentation performance improved, reaching its peak at approximately $\epsilon = 0.08$. However, beyond this optimal point, the performance started to decline, indicating that stronger perturbations can enhance the model’s performance only within a certain range. In this work, by precisely defining the acceptable range of perturbations, we restrict the pertur-

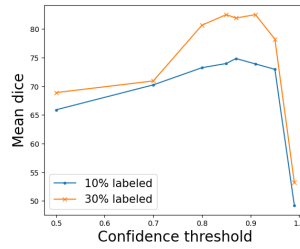


Figure 5. Mean Dice score produced by varying the confidence threshold for pseudo-labels

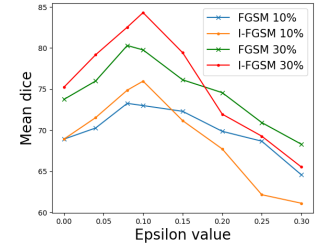


Figure 6. Optimal ϵ value enhances segmentation performance (as indicated by the peak in mean Dice score)

bations within the ϵ -neighbourhood, which ensures that the integrity of the instrument pixels is preserved while introducing subtle variations that aid in improved generalization of the model. Comparing FGSM and I-FGSM, we found that I-FGSM showed superior performance to FGSM before reaching the optimal ϵ value. However, after the optimal point, I-FGSM exhibited a more significant decrease in the model’s performance compared to FGSM, which suggests that I-FGSM has a higher attack success rate than FGSM but becomes more harmful to the model when the attacking amplitude is large. We also varied the number of I-FGSM iterations as shown in Table 4 and qualitatively illustrated in Figure 7. Increasing the number of iterations in the I-FGSM attack shows a minor improvement consistent with expectations that it increases the attack success rate. However, it is important to consider that this small improvement in segmentation performance through increased iterations comes with a trade-off in computational efficiency.

We also conducted experiments using various adversarial learning methods as shown in Table 4. Our findings

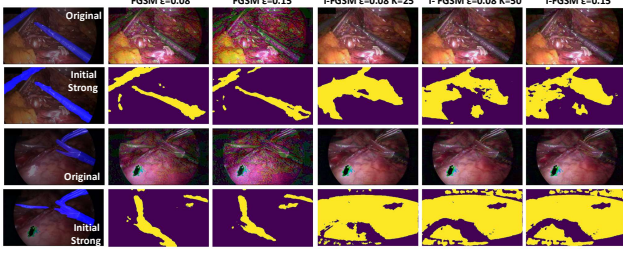


Figure 7. Examples showcase the impact of strong augmentation transform functions and adversarial augmentation on an original unlabelled image input to a model. The first column features the original image covered by its segmentation mask output from the model, as well as the strongly-augmented image obtained via initial strong augmentation and its output segmentation mask. The 2-6 columns showcase adversarial images produced by I-FGSM with varying values of ϵ and K (which becomes FGSM when $K = 0$) to replace the original strongly-augmented images for model parameter updating. The upper rows in the 2-6 columns display the adversarial images, while the bottom rows show the corresponding segmentation results produced by the model.

indicate that performance achieved by using one-step attack methods is consistently lower compared to our iterative strategy, which suggests when attempting to manipulate image samples to create adversarial examples, breaking the attack down into smaller steps can improve the overall success rate, as noted in previous research [21].

Table 4. Segmentation performance of SegMatch on Robust-MIS 2019 when applying different adversarial attack methods

| Adversarial Method | Labelled: 1794(30%) | |
|--------------------------------------|---------------------|------|
| | Mean Dice | NSD |
| C&W [5] | 72.9 | 70.4 |
| FGSM [46] | 75.8 | 79.6 |
| DDN [36] | 78.9 | 77.2 |
| I-FGSM ($\epsilon = 0.08, K = 25$) | 84.3 | 80.2 |
| I-FGSM ($\epsilon = 0.08, K = 50$) | 84.9 | 81.5 |

6. Conclusion

In this paper, we introduced SegMatch, a semi-supervised learning algorithm for surgical tool segmentation that achieves state-of-the-art results across two of the most commonly used datasets in this field. Our algorithm, SegMatch, was adapted from a simple semi-supervised classification algorithm FixMatch which combines consistency regularization and pseudo-labelling. During training, SegMatch makes use of a standard labelled image pathway and an unlabelled image pathway with training batches mixing labelled and unlabelled images. The unlabelled image pathway is composed of two concurrent

branches. A weak augmentation branch is used to generate pseudo-labels against which the output of a strong augmentation branch is compared. Considering the limitation of fixed handcrafted strongly augmentation techniques, we introduced adversarial augmentations to increase the performance of strongly augmented images. We also highlighted the importance of considering equivariance and invariance properties in the augmentation functions used for segmentation. Putting our work into its application context, automatic visual understanding is critical for advanced surgical assistance but labelled data to train supporting algorithms are expensive and difficult to obtain. We believe that simple but strong-performance semi-supervised segmentation learning algorithms, such as our proposed SegMatch, will accelerate the deployment of surgical instrument segmentation in the operating theatre.

References

- [1] Max Allan, Alex Shvets, Thomas Kurmann, Zichen Zhang, Rahul Duggal, Yun-Hsuan Su, Nicola Rieke, Iro Laina, Niveditha Kalavakonda, Sebastian Bodenstedt, et al. 2017 robotic instrument segmentation challenge. *arXiv preprint arXiv:1902.06426*, 2019. 2, 6
- [2] Antreas Antoniou, Amos Storkey, and Harrison Edwards. Data augmentation generative adversarial networks. *arXiv preprint arXiv:1711.04340*, 2017. 3
- [3] David Berthelot, Nicholas Carlini, Ekin D Cubuk, Alex Kurakin, Kihyuk Sohn, Han Zhang, and Colin Raffel. Remixmatch: Semi-supervised learning with distribution alignment and augmentation anchoring. *arXiv preprint arXiv:1911.09785*, 2019. 5
- [4] David Berthelot, Nicholas Carlini, Ian Goodfellow, Nicolas Papernot, Avital Oliver, and Colin A Raffel. Mixmatch: A holistic approach to semi-supervised learning. *Advances in neural information processing systems*, 32, 2019. 2, 4, 5
- [5] Nicholas Carlini and David Wagner. Towards evaluating the robustness of neural networks. In *2017 IEEE Symposium on Security and Privacy (SP)*, pages 39–57. Ieee, 2017. 3, 10
- [6] Liang-Chieh Chen, Raphael Gontijo Lopes, Bowen Cheng, Maxwell D Collins, Ekin D Cubuk, Barret Zoph, Hartwig Adam, and Jonathon Shlens. Naive-student: Leveraging semi-supervised learning in video sequences for urban scene segmentation. In *European Conference on Computer Vision*, pages 695–714. Springer, 2020. 2
- [7] Xiaokang Chen, Yuhui Yuan, Gang Zeng, and Jingdong Wang. Semi-supervised semantic segmentation with cross pseudo supervision. In *Proceedings of the IEEE/CVF Conference on Computer Vision and Pattern Recognition*, pages 2613–2622, 2021. 2
- [8] Jeremy Cohen, Elan Rosenfeld, and Zico Kolter. Certified adversarial robustness via randomized smoothing. In *International Conference on Machine Learning*, pages 1310–1320. PMLR, 2019. 3
- [9] Ekin D Cubuk, Barret Zoph, Jonathon Shlens, and Quoc V Le. Randaugment: Practical automated data augmentation with a reduced search space. In *Proceedings of*

- the *IEEE/CVF conference on computer vision and pattern recognition workshops*, pages 702–703, 2020. 4, 5, 7
- [10] Zhengyang Feng, Qianyu Zhou, Qiqi Gu, Xin Tan, Guangliang Cheng, Xuequan Lu, Jianping Shi, and Lizhuang Ma. Dmt: Dynamic mutual training for semi-supervised learning. *Pattern Recognition*, page 108777, 2022. 2
- [11] Luis C Garcia-Peraza-Herrera, Lucas Fidon, Claudia D’Ettorre, Danail Stoyanov, Tom Vercauteren, and Sebastien Ourselin. Image compositing for segmentation of surgical tools without manual annotations. *IEEE transactions on medical imaging*, 40(5):1450–1460, 2021. 5
- [12] Cristina González, Laura Bravo-Sánchez, and Pablo Arbelaez. Isinet: an instance-based approach for surgical instrument segmentation. In *International Conference on Medical Image Computing and Computer-Assisted Intervention*, pages 595–605. Springer, 2020. 3, 6, 8, 9
- [13] Ian Goodfellow, Jean Pouget-Abadie, Mehdi Mirza, Bing Xu, David Warde-Farley, Sherjil Ozair, Aaron Courville, and Yoshua Bengio. Generative adversarial nets. In Z. Ghahramani, M. Welling, C. Cortes, N. Lawrence, and K.Q. Weinberger, editors, *Advances in Neural Information Processing Systems*, volume 27. Curran Associates, Inc., 2014. 3
- [14] Yves Grandvalet and Yoshua Bengio. Semi-supervised learning by entropy minimization. *Advances in neural information processing systems*, 17, 2004. 2
- [15] SM Kamrul Hasan and Cristian A Linte. U-netplus: A modified encoder-decoder u-net architecture for semantic and instance segmentation of surgical instruments from laparoscopic images. In *2019 41st annual international conference of the IEEE engineering in medicine and biology society (EMBC)*, pages 7205–7211. IEEE, 2019. 1
- [16] Geoffrey Hinton, Oriol Vinyals, Jeff Dean, et al. Distilling the knowledge in a neural network. *arXiv preprint arXiv:1503.02531*, 2(7), 2015. 3
- [17] Fabian Isensee and Klaus H Maier-Hein. Or-unet: an optimized robust residual u-net for instrument segmentation in endoscopic images. *arXiv preprint arXiv:2004.12668*, 2020. 1, 7, 8, 9
- [18] Mobarakol Islam, Yueyuan Li, and Hongliang Ren. Learning where to look while tracking instruments in robot-assisted surgery. In *International Conference on Medical Image Computing and Computer-Assisted Intervention*, pages 412–420. Springer, 2019. 1, 3
- [19] Yueming Jin, Keyun Cheng, Qi Dou, and Pheng-Ann Heng. Incorporating temporal prior from motion flow for instrument segmentation in minimally invasive surgery video. In *International Conference on Medical Image Computing and Computer-Assisted Intervention*, pages 440–448. Springer, 2019. 3
- [20] Jongmok Kim, Jooyoung Jang, and Hyunwoo Park. Structured consistency loss for semi-supervised semantic segmentation. *arXiv preprint arXiv:2001.04647*, 2020. 2
- [21] Alexey Kurakin, Ian J Goodfellow, and Samy Bengio. Adversarial examples in the physical world. In *Artificial intelligence safety and security*, pages 99–112. Chapman and Hall/CRC, 2018. 2, 3, 5, 10
- [22] Iro Laina, Nicola Rieke, Christian Rupprecht, Josué Page Vizcaíno, Abouzar Eslami, Federico Tombari, and Nassir Navab. Concurrent segmentation and localization for tracking of surgical instruments. In *International conference on medical image computing and computer-assisted intervention*, pages 664–672. Springer, 2017. 1
- [23] Samuli Laine and Timo Aila. Temporal ensembling for semi-supervised learning. *arXiv preprint arXiv:1610.02242*, 2016. 6
- [24] Xiaomeng Li, Lequan Yu, Hao Chen, Chi-Wing Fu, and Pheng-Ann Heng. Semi-supervised skin lesion segmentation via transformation consistent self-ensembling model. *arXiv preprint arXiv:1808.03887*, 2018. 2
- [25] Daochang Liu, Yuhui Wei, Tingting Jiang, Yizhou Wang, Rulin Miao, Fei Shan, and Ziyu Li. Unsupervised surgical instrument segmentation via anchor generation and semantic diffusion. In *International Conference on Medical Image Computing and Computer-Assisted Intervention*, pages 657–667. Springer, 2020. 2, 3
- [26] Jie Liu, Xiaoqing Guo, and Yixuan Yuan. Graph-based surgical instrument adaptive segmentation via domain-common knowledge. *IEEE Transactions on Medical Imaging*, 41(3):715–726, 2021. 3
- [27] Aleksander Madry, Aleksandar Makelov, Ludwig Schmidt, Dimitris Tsipras, and Adrian Vladu. Towards deep learning models resistant to adversarial attacks. *arXiv preprint arXiv:1706.06083*, 2017. 3
- [28] Fausto Milletari, Nicola Rieke, Maximilian Baust, Marco Esposito, and Nassir Navab. Cfcm: segmentation via coarse to fine context memory. In *International Conference on Medical Image Computing and Computer-Assisted Intervention*, pages 667–674. Springer, 2018. 1, 3
- [29] Shervin Minaee, Yuri Boykov, Fatih Porikli, Antonio Plaza, Nasser Kehtarnavaz, and Demetri Terzopoulos. Image segmentation using deep learning: A survey. *IEEE transactions on pattern analysis and machine intelligence*, 44(7):3523–3542, 2021. 5
- [30] Yassine Ouali, Céline Hudelot, and Myriam Tami. Semi-supervised semantic segmentation with cross-consistency training. In *Proceedings of the IEEE/CVF Conference on Computer Vision and Pattern Recognition*, pages 12674–12684, 2020. 2, 7, 9
- [31] George Papandreou, Liang-Chieh Chen, Kevin P Murphy, and Alan L Yuille. Weakly-and semi-supervised learning of a deep convolutional network for semantic image segmentation. In *Proceedings of the IEEE international conference on computer vision*, pages 1742–1750, 2015. 7, 9
- [32] Siyuan Qiao, Wei Shen, Zhishuai Zhang, Bo Wang, and Alan Yuille. Deep co-training for semi-supervised image recognition. In *Proceedings of the european conference on computer vision (eccv)*, pages 135–152, 2018. 2
- [33] Fangbo Qin, Yangming Li, Yun-Hsuan Su, De Xu, and Blake Hannaford. Surgical instrument segmentation for endoscopic vision with data fusion of cnn prediction and kinematic pose. In *2019 international conference on robotics and automation (ICRA)*, pages 9821–9827. IEEE, 2019. 3
- [34] Antti Rasmus, Mathias Berglund, Mikko Honkala, Harri Valpola, and Tapani Raiko. Semi-supervised learning with ladder networks. *Advances in neural information processing systems*, 28, 2015. 2

- [35] Nicola Rieke, David Joseph Tan, Chiara Amat di San Filippo, Federico Tombari, Mohamed Alsheakhali, Vasileios Belagiannis, Abouzar Eslami, and Nassir Navab. Real-time localization of articulated surgical instruments in retinal microsurgery. *Medical image analysis*, 34:82–100, 2016. [1](#)
- [36] Jérôme Rony, Luiz G Hafemann, Luiz S Oliveira, Ismail Ben Ayed, Robert Sabourin, and Eric Granger. Decoupling direction and norm for efficient gradient-based l2 adversarial attacks and defenses. In *Proceedings of the IEEE/CVF Conference on Computer Vision and Pattern Recognition*, pages 4322–4330, 2019. [3](#), [10](#)
- [37] Tobias Ross, Annika Reinke, Peter M Full, Martin Wagner, Hannes Kenngott, Martin Apitz, Hellena Hempe, Diana Mindroc Filimon, Patrick Scholz, Thuy Nuong Tran, et al. Robust medical instrument segmentation challenge 2019. *arXiv preprint arXiv:2003.10299*, 2020. [1](#), [2](#), [6](#), [7](#), [9](#)
- [38] Tobias Ross, David Zimmerer, Anant Vemuri, Fabian Isensee, Manuel Wiesenfarth, Sebastian Bodenstedt, Fabian Both, Philip Kessler, Martin Wagner, Beat Müller, et al. Exploiting the potential of unlabeled endoscopic video data with self-supervised learning. *International journal of computer assisted radiology and surgery*, 13(6):925–933, 2018. [2](#)
- [39] Manish Sahu, Anirban Mukhopadhyay, and Stefan Zachow. Simulation-to-real domain adaptation with teacher–student learning for endoscopic instrument segmentation. *International Journal of Computer Assisted Radiology and Surgery*, 16(5):849–859, 2021. [2](#), [3](#)
- [40] Pouya Samangouei, Maya Kabkab, and Rama Chellappa. Defense-gan: Protecting classifiers against adversarial attacks using generative models. *arXiv preprint arXiv:1805.06605*, 2018. [3](#)
- [41] Ricardo Sanchez-Matilla, Maria Robu, Imanol Luengo, and Danail Stoyanov. Scalable joint detection and segmentation of surgical instruments with weak supervision. In *International Conference on Medical Image Computing and Computer-Assisted Intervention*, pages 501–511. Springer, 2021. [2](#), [3](#)
- [42] Lalithkumar Seenivasan, Sai Mitheran, Mobarakol Islam, and Hongliang Ren. Global-reasoned multi-task learning model for surgical scene understanding. *IEEE Robotics and Automation Letters*, 7(2):3858–3865, 2022. [3](#)
- [43] Kihyuk Sohn, David Berthelot, Nicholas Carlini, Zizhao Zhang, Han Zhang, Colin A Raffel, Ekin Dogus Cubuk, Alexey Kurakin, and Chun-Liang Li. Fixmatch: Simplifying semi-supervised learning with consistency and confidence. *Advances in Neural Information Processing Systems*, 33:596–608, 2020. [2](#), [3](#), [5](#)
- [44] Nasim Souly, Concetto Spampinato, and Mubarak Shah. Semi supervised semantic segmentation using generative adversarial network. In *Proceedings of the IEEE international conference on computer vision*, pages 5688–5696, 2017. [2](#)
- [45] Stefanie Speidel, Enrico Kuhn, Sebastian Bodenstedt, Sebastian Röhl, Hannes Kenngott, B Müller-Stich, and Rüdiger Dillmann. Visual tracking of da vinci instruments for laparoscopic surgery. In *Medical Imaging 2014: Image-Guided Procedures, Robotic Interventions, and Modeling*, volume 9036, pages 47–52. SPIE, 2014. [1](#)
- [46] Christian Szegedy, Wojciech Zaremba, Ilya Sutskever, Joan Bruna, Dumitru Erhan, Ian Goodfellow, and Rob Fergus. Intriguing properties of neural networks. *arXiv preprint arXiv:1312.6199*, 2013. [3](#), [10](#)
- [47] Antti Tarvainen and Harri Valpola. Mean teachers are better role models: Weight-averaged consistency targets improve semi-supervised deep learning results. *Advances in neural information processing systems*, 30, 2017. [2](#), [7](#), [9](#)
- [48] Florian Tramèr, Alexey Kurakin, Nicolas Papernot, Ian Goodfellow, Dan Boneh, and Patrick McDaniel. Ensemble adversarial training: Attacks and defenses. *arXiv preprint arXiv:1705.07204*, 2017. [3](#)
- [49] Qizhe Xie, Minh-Thang Luong, Eduard Hovy, and Quoc V Le. Self-training with noisy student improves imagenet classification. In *Proceedings of the IEEE/CVF conference on computer vision and pattern recognition*, pages 10687–10698, 2020. [2](#)
- [50] Zixu Zhao, Yueming Jin, Xiaojie Gao, Qi Dou, and Pheng-Ann Heng. Learning motion flows for semi-supervised instrument segmentation from robotic surgical video. In *International Conference on Medical Image Computing and Computer-Assisted Intervention*, pages 679–689. Springer, 2020. [2](#)